SCIENCE CHINA
Earth Sciences

• RESEARCH PAPER •

July 2015 Vol.58 No.7: 1133–1147
doi: 10.1007/s11430-015-5094-6

Crustal velocity structure in the Emeishan large igneous province and evidence of the Permian mantle plume activity

XU Tao[1,2*], ZHANG ZhongJie[1], LIU BaoFeng[3], CHEN Yun[1], ZHANG MingHui[1,4], TIAN XiaoBo[1,2], XU YiGang[5] & TENG JiWen[1]

[1] *State Key Laboratory of Lithospheric Evolution, Institute of Geology and Geophysics, Chinese Academy of Sciences, Beijing 100029, China;*
[2] *CAS Center for Excellence in Tibetan Plateau Earth Sciences, Beijing 100101, China;*
[3] *Geophysical Exploration Center, China Earthquake Administration, Zhengzhou 450002, China;*
[4] *University of Chinese Academy of Sciences, Beijing 100049, China;*
[5] *State Key Laboratory of Isotope Geochemistry, Guangzhou Institute of Geochemistry, Chinese Academy of Sciences, Guangzhou 510640, China*

Received February 9, 2015; accepted April 9, 2015; published online April 29, 2015

The Emeishan large igneous province (ELIP) in SW China is interpreted to be associated with an ancient mantle plume. Most of the constraints on the role of mantle plume in the generation of the Emeishan flood basalts were provided by geological and geochemical methods, but the geophysical investigation is very limited. In order to better understand the deep structure and features of ELIP, we have studied the crustal velocity structure using the data acquired from the Lijiang-Panzhihua-Qingzhen wide-angle seismic profile. This profile crosses the three sub-zones of the ELIP (the inner, intermediate, and outer zones), divided based on the differential erosion and uplift of the Maokou limestone. The results provided by the active source seismic experiment demonstrate: (1) The average depth of the crystalline basement along the profile is about 2 km. (2) The middle crust in the Inner Zone is characterized by high-velocity anomalies, with the average velocity of 6.2–6.6 km/s, which is about 0.1– 0.2 km/s higher than the normal one. The velocity of the lower crust in the inner zone is 6.9–7.2 km/s, higher than those observed in the intermediate and outer zones (6.7–7.0 km/s). Relatively low velocity anomalies appear in the upper, middle and lower crusts near the junction of the inner zone and intermediate zone, probably due to the effect of the Xiaojiang fault (XJF). (3) The average velocity of the crust is comparatively low on both sides of XJF, especially on the east side, and the average velocity of the consolidated continental crust is also low there. This may suggest that the XJF extends at least down to 40 km deep, even beyond through the crust. (4) The depth to the Moho discontinuity decrease gradually from 47–53 km in the inner zone, via 42–50 km in the intermediate zone to 38–42 km in the outer zone. In the inner zone, the Moho uplifts locally and the (consolidated) crust is characterized by high-velocity anomalies, which are likely related to intensive magma intrusion and underplating associated with melting of plume head. Overall the crustal velocity structure in the study area recorded the imprint left by the Permian Emeishan mantle plume.

Emeishan large igneous province, Permian mantle plume, wide-angle seismic reflection/refraction data, Lijiang-Panzhihua-Qingzhen profile, crustal velocity

Citation: Xu T, Zhang Z J, Liu B F, Chen Y, Zhang M H, Tian X B, Xu Y G, Teng J W. 2015. Crustal velocity structure in the Emeishan large igneous province and evidence of the Permian mantle plume activity. Science China: Earth Sciences, 58: 1133−1147, doi: 10.1007/s11430-015-5094-6

*Corresponding author (email: xutao@mail.iggcas.ac.cn)

Large Igneous Provinces (LIPs) characterized by voluminous volcanic sequences erupted in a short period of time (generally several million years) are magmatic formation composed of ultramafic extrusive rocks and intrusive rocks (Richards et al., 1989; Campbell and Griffiths, 1990; Coffin and Eldholm, 1994; Xu, 2002; Xia et al., 2004; Zhang and Dong, 2007). As the largest magmatism on Earth scale, the LIPs recorded the transfer of massive material and energy from the interior to the exterior of the Earth at a certain historical period. Recently, recognition of the potential role of LIPs in affecting the earth surface topography, the mass extinction, and the formation of regional vast mineral resources has led to an increased interest in the geoscience field (Campbell and Griffiths, 1990; Chung and Jahn, 1995; Xu and Chung, 2001; Xu Y G et al., 2001, 2004, 2007a, 2007b, 2013; Ali et al., 2005; Lo et al., 2002; Zhu et al, 2002; Xu, 2002; He et al., 2003a, 2003b, 2005, 2006a, 2006b, 2007).

Mantle plumes can be divided into modern and ancient mantle plumes depending on their formation time. The Emeishan large igneous province (hereafter ELIP) erupted at ~259 Ma is an important large igneous province in China (Mathoney and Coffin, 1997; Courtillot et al., 1999; Xu and Chung, 2001; Xu et al., 2013). The formation of the ELIP is generally considered as a result of an ancient mantle plume (Chung and Jahn, 1995; He et al., 2003a, 2003b, 2005, 2006a, 2006b, 2007; Xu Y G et al., 2004; Zhang et al., 2006b; Wu and Zhang, 2012). The eruption of massive magmas may have caused important changes in the global climate and environment and the extinction events in the Late Permian. Hence ELIP has attracted a growing interest among the scholars (Chung and Jahn, 1995; Xu and Chung, 2001; Zhang et al., 2006a; Ali et al., 2005; Xu Y G et al., 2001, 2004, 2007b, 2013; He et al., 2003a, 2003b, 2005, 2006a, 2006b, 2007; Peate and Bryan, 2008; Wignall et al., 2009; Zhang Y et al., 2013; Wu et al., 2014).

Geophysics is the main method to identify the modern mantle plumes, as it provides us with a present snapshot of the structure of the Earth (Courtillot et al., 2003; Lei and Zhao, 2006). The geophysical approach encounters its difficulty in identifying ancient plumes, because the anomalous thermal structure in the interior of the ancient mantle plumes no longer exists, and it is rather difficult to correlate spatially the surface structure with the deep structure due to the tectonic movements after the LIPs' formation (Xu Y G et al., 2004, 2007b; Wu and Zhang, 2012). Campbell (2001) listed five criteria related to geological and geochemical aspects to identify the ancient mantle plumes: prevolcanic uplift, radiating dyke swarm, physical volcanology, hotspot tracks, and geochemical characteristics of plume-derived basalts. The EILP meets three to four of these aspects (Xu et al., 2013). Therefore, an ancient mantle plume model has been proposed to explain the formation of the ELIP (He et al., 2003a, 2006a, 2007; Xu Y G et al., 2004, 2007b; Zhang et al., 2006b).

In this study, we try to use the geophysical approach to identify the imprints left by the ancient mantle plume. The volcanism generated by the ancient mantle plumes would lead to thermal anomalies in the crust and the mantle lithosphere, and also to the intrusion and eruption of magmas, so that the material composition of the crust and mantle would change correspondingly, which are the imprints of the events provoked by ancient mantle plumes. These imprints can be recognized by comparing variations of the seismic velocity, V_p/V_s ratio, density, anisotropy, rheology, and magnetism with the properties in the surrounding areas. The variations of the petrophysical properties in the lithospheric mantle and especially in the crust will hardly experience significant changes with time since there are no apparent effects from the heat-induced tectonic movements. In order to provide geophysical constraints on the variations of the physical properties of the crust and uppermost mantle in ELIP, we have determined the crust-mantle seismic velocity structure on the basis of the data acquired in the course of the COMWIDE-ELIP seismic experiment, which consists of an active-source seismic sounding performed across the study area, along the Lijiang-Qingzhen profile.

1 Tectonic setting

The ELIP is located at the western margin of the Yangtze Craton, SW China. The Emeishan basalts are exposed in a rhombus-shaped province of 2.5×10^5 km^2 bounded by the Ailaoshan-Red River slip fault in the southwest (Figure 1) and the Longmenshan thrust fault in the northwest (Xu and Chung, 2001; Xu Y G et al., 2001, 2004, 2007a, 2007b, 2013; He et al., 2003a, 2007; Peate and Bryan, 2008; Wu and Zhang, 2012; Zhang Y et al., 2013). The province consists of dominant basaltic lavas and subordinate pyroclastic rocks, which were emplaced mainly at ~259 Ma (Zhou et al., 2002; Zhong et al., 2014). Since then the ELIP has been subjected to the Indosinian and Yanshanian movements. Since the Cenozoic era, the Emeishan basalts have been affected by the interaction of the material flow eastward within the Tibet plateau and the intrusion of the Assam vertex (Armijo et al., 1989; Qiao et al., 2004; Chen et al., 2013). The ELIP has suffered strong deformation and the destruction of the history of complex tectonic movements, masking partially the original distribution of the basalts.

The Maokou Formation underlies the Emeishan basalts, and the contact between them is an unconformity. Through the biostratigraphic comparison and sedimentologic features of the Maokou limestone in SW China, He et al. (2003a, 2003b) suggested differential erosion took place prior to the eruption of the Emeishan flood basalts and the erosional extent changing regularly in space. According to the extent of the erosion of the Maokou Formation, the ELIP is divided into three zones: the inner, intermediate, and outer zones (Figure 1) (He et al., 2003a, 2003b; Xu Y G et al., 2004,

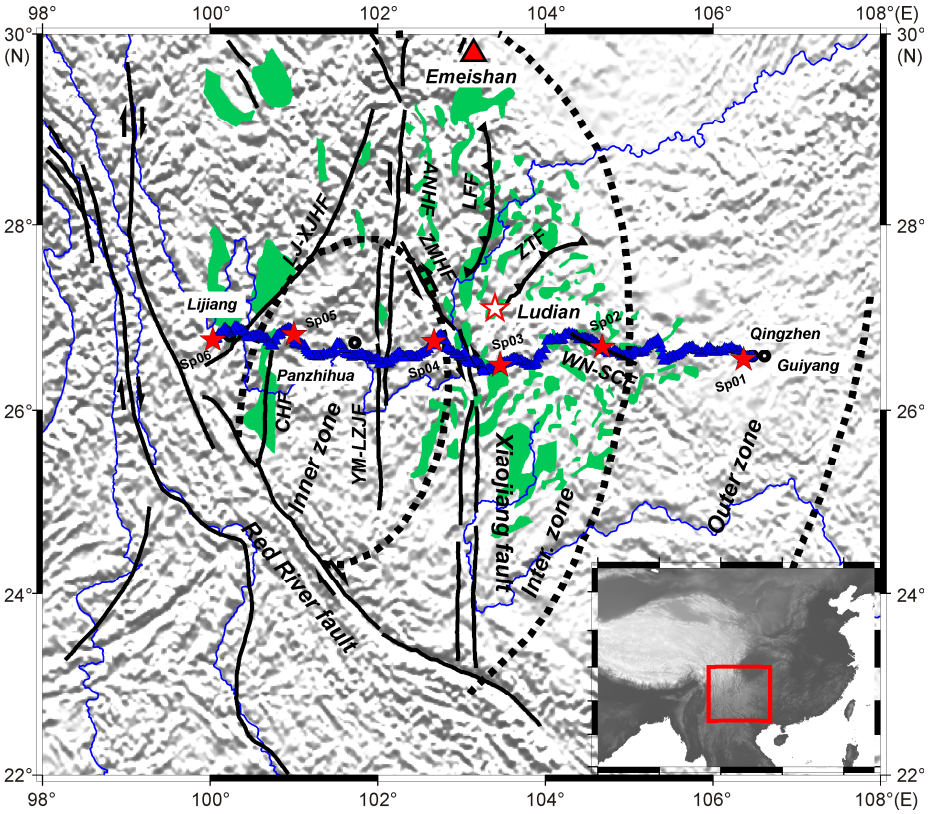

Figure 1 Map of the Emeishan large igneous province (ELIP) showing the distribution of basalts (in green color) and the west-east trending active-source seismic array between Lijiang-Qingzhen used in this study. Red stars mark shot points, and blue triangles indicate receivers. The hollow red star indicated the epicentral location of the M_s 6.5 Ludian earthquake occurred in 2014. The dashed lines outline the boundaries between the inner, intermediate and outer zones of ELIP. RRF, Red River fault; XJF, Xiaojiang fault; LJ-XJHF, Lijiang-Xiaojinhe fault; CHF, Chenghai fault; YM-LZJF, Yuanmou-Lüzhijiang fault; ANHF, Anninghe fault; ZMHF, Zemuhe fault; LFF, Lianfeng fault; ZTF, Zhaotong fault; WN-SCF, Weining-Shuicheng fault.

2007b). The inner zone with a diameter of about 400 km, where the Maokou Formation was strongly eroded, encloses the west of Yunnan and the south of Sichuan. The thickness of the remaining Maokou Formation is usually less than 100 m, mostly about 50 m. The Maokou Formation was partly eroded and its thickness increases to 200–450 m in the intermediate zone, which includes a large part of the east of Yunnan and north Sichuan. The thickness of the Maokou Formation in the outer zone, where the erosion was generally weak, is 250–600 m approximately. There is a short sedimentary hiatus between the Maokou limestone and the Emeishan basalts in this zone.

The 650-km-long profile between Lijiang and Qingzhen is an active-source seismic sounding oriented in EW direction across the ELIP, which begins at Lijiang, Yunnan province, passes by Panzhihua, and arrives up to Qingzhen in Guizhou province (Figure 1). The profile has an elevation of about 1500–2000 m and is located on the Yunnan-Guizhou-Sichuan plateau. The geological structures along the profile are complex and are mostly eroded mountain lands. There is an incomplete stratigraphic series of Quaternary deposits along the survey line, but the Early-Middle Triassic and Middle-Upper Devonian sedimentary strata and the continental flood basalts are widely distributed.

The Lijiang-Qingzhen profile crosses several main faults from west to east: Lijiang-Xiaojinhe fault (LJ-XJHF), Chenghai fault (CHF), Yuanmou-Lüzhijiang fault (YM-LZJF), Anninghe fault (ANHF), Xiaojiang fault (XJF), and Weining-Shuicheng fault (WN-SCF) (Figure 1). LJ-XJHF in NS direction is an active sinistral strike-slip fault (Xiang et al., 2002). CHF is about 200 km long from Ninglang in the north to Midu in the south. The ultrabasic rocks are distributed sporadically along CHF. YM-LZJF with the NS trend is a major active fracture in the Sichuan-Yunnan region and is the dominant fault in the basin located in the central region (Bai and Wang, 2003). ANHF is an important strike-slip fault that borders between Tibet and the South China block (He and Yasutakyr, 2007). XJF with a trend nearly in NS direction is a large active fault, whose south segment intersects the Qujiang fault and the Honghe fault which are in NW direction, thus constructing a special and complex wedge block structure (He et al. 1993; Yu et al., 1997). WN-SCF is located in the region of Weining-Shuicheng in Guizhou. It is the boundary of the stratigraphic district in central and northwestern Guizhou (Zhang et al., 2009).

2 Data acquisition and seismic phases

2.1 Data acquisition

In June 2012 the Institute of Geology and Geophysics, Chinese Academy of Sciences, carried out six explosions along the Lijiang-Panzhihua-Qingzhen profile nearly in EW direction; the amount of explosives reached up to 17.5 tons TNT, while the amount of a single shot was about 2.4–3.9 tons. The combined underground blasting was designed to be the shooting mode, and the shots were spaced 60–90 km. The in-line profile was extended approximately 650 km in length and 323 portable digital seismographs stations were spaced 1.5–2.0 km and deployed to record the field data (Figure 1).

2.2 Analysis of seismic phases

Seismic phases identified include Pg, Pm, Pc, and Pn phases. Pg is the refracted seismic phase from the crystalline basement in the shallow crust and makes up the first arrivals; Pm is the strongly reflected phase from the Moho discontinuity; Pn is the refracted phase from the weak velocity gradient layer in the uppermost mantle, with an apparent velocity of about 8.0–8.1 km/s. The reflected phases from the second-order velocity discontinuity within the crust are waves with relatively weak energies, and are collectively known as the Pc phase. There are mainly three groups of intra-crustal reflection phases, which are denoted usually as P1, P2, and P3 to increasing depths.

2.2.1 First arrivals

The first-arrivals of Pg are recorded at offsets from tens to more than one hundred kilometers. The apparent velocity near the shots increases rapidly and then is stabilized at 6.0–6.3 km/s with the increase of the offset. The travel time curves of the Pg phases reflect the thickness of the sedimentary cover and the velocity structure of the crystalline basement. The advance or delay of the local travel times is generally related with local uplifts and depressions of the surface.

The first arrivals corresponding to Pg phases generated by the 6 shots along the Lijiang-Qingzhen profile can be correlated about 60–120 km in EW direction and they all are clear and have high signal-to-noise ratio (Figures 2–7). The reduced travel time is calculated using the reduction velocity of 6.0 km/s, and its value is about 0.5 s at 60 km along the profile, where the Pg seismic phase presents nearly horizontal and hence its apparent velocity is near 6.0 km/s.

A preliminary indication of the results from the Pg phases is that the shallow covering layer along the profile is not too thick and the velocity is up to 4.0 km/s. Based on the picked first-arrival Pg phases from the six shots, the velocity structure of the upper crust is inverted by the finite difference method (Vidale, 1988; Hole, 1992; Zhao et al., 2004; Lan and Zhang, 2013a, 2013b; Lan et al., 2012a, 2012b; Liu et al., 2012; Zhao et al., 2014; Ma and Zhang, 2014). The velocity structure of the upper crust so determined can be considered as the initial model of the shallow crust that is used to then invert the crustal velocity structure (Xu et al., 2014a).

2.2.2 Later arrivals

Compared with the first arrivals, which are clear and easy to be traced, the later arrivals, such as Pc, Pm, and Pn are characterized by low signal-to-noise ratio due to the thick Moho in the Yunnan-Guizhou-Sichuan region (Xiong et al., 1993; Teng, 1994; Liu et al., 2001; Wang et al., 2002; Bai and Wang, 2003; Chen et al., 2010; Sun et al., 2012; Zhou et al., 2012; Zhang E H et al., 2013; Zhang Z J et al., 2013; Teng et al., 2013). Taking the Moho depth in this region as the reference, the later arrivals are traced by the exchange principle of the travel times of the seismic phases between two shots. The results are shown in Figures 2–7.

Generally speaking, the intercepts of the travel time curves of the seismic phases, which are the picked reduced travel times, mainly reflect the depth of the reflection interfaces. The Moho depth becomes deeper as the reduced travel time of Pm phase increases. The curve slopes of the seismic phases mainly reflect the average velocities of the strata above the Moho. For Pm phases, a large offset may lead to a total reflection and the apparent velocity at this offset is approximated to the velocity of the lower crust at the reflection point. Let us see the Pm phases reflected from the Moho discontinuity as examples: from east to west, on the left side of the first shot (Figure 2(a)), the reduced travel time of Pm phase is about 2.3 s at offset of 150 km and no phases are traced around an offset of 200 km; on the left of the second shot (Figure 3(a)), the reduced travel time of Pm phase is about 3.3 s at offset of 150 km and no phases are traced around the offset of 200 km; on the left of the third shot (Figure 4(a)), the reduced travel time of Pm phase is 2.2 s at offset of 200 km, and no phases are traced at offset of 150 km; on the left of the fourth shot (Figure 5(a)), the reduced travel time of Pm phase is about 2.7 s at offset 150 km. From east to west, the reduced travel times of the Pm phases increase gradually and then decrease, which indicates that the Moho discontinuity along the profile is gradually deeper and then becomes shallower.

By correcting the structural model many times and using forward calculation by ray tracing to calculate the travel times of multi-phases (Cerveny et al., 1988; Vidale, 1988; Zelt and Smith, 1992; Cerveny, 2001; Xu T et al., 2004; Xu et al., 2006, 2010, 2014b; Li et al., 2013; Lan et al., 2013a, 2013b), we obtained the final crust-mantle model. The identification of seismic phases has a great impact on the velocity structure and therefore the geophysical model for the study region needs to be the most accurate possible to adequately constrain the medium. The depth error of an interface is about ±1 km and the velocity error is about ±0.1 km/s. In Figures 2–7 we show original seismograms and

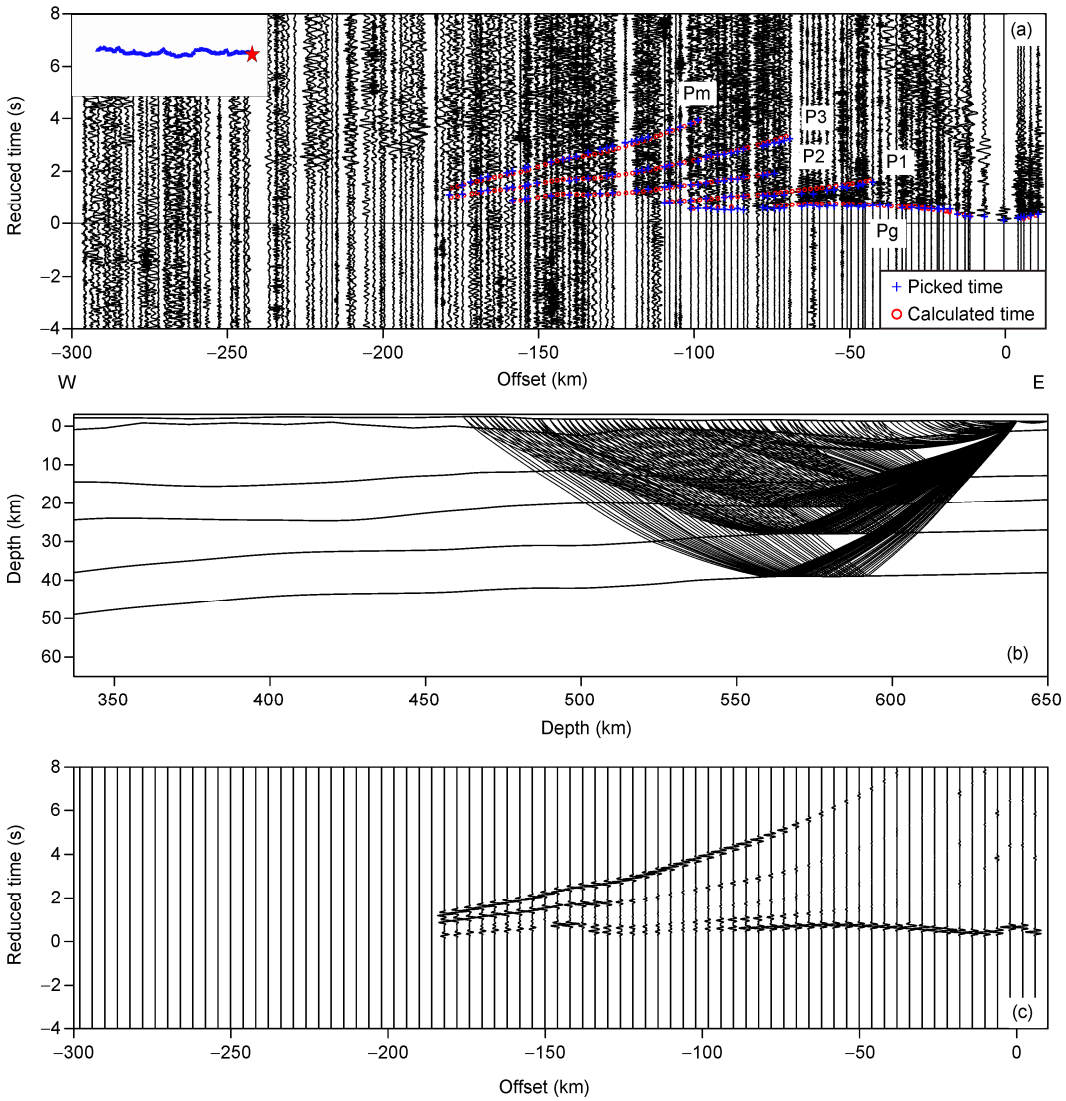

Figure 2 Shot point Sp01 of the Lijiang-Qingzhen profile. (a) Original seismograms and multiple P-phases picked for analysis (blue crosses) and calculated travel times (red circles); (b) seismic interfaces and ray diagram; (c) synthetic seismograms. A velocity of 6.0 km/s was used for reduced time.

multiple P-phases picked for analysis and also computed travel times; seismic interfaces and ray diagrams; and synthetic seismograms.

2.3 Travel time fitting and ray coverage

The fit between observed and calculated travel times for all P-phases recorded from the 6 shots fired along the Lijiang-Qingzhen profile reveals a good agreement (Figure 8). Furthermore, the ray coverage diagram is rather dense and allows seeing a good illumination of the crust (Figure 9). These two facts result in a reliable velocity structure.

3 Seismic velocity structure

3.1 2D velocity structure

The 2D velocity structure of the crust along the Lijiang-Qingzhen profile is shown in Figure 10 (lower panel). Intracrustal reflectors (P1, P2, and P3) and the Moho discontinuity are drawn following the reflection points of the ray paths (small circles). The crust is divided approximately into upper crust (from the surface to P1), middle crust (from P1 to P3), and lower crust (from P3 to the Moho discontinuity). The shallowest layers are characterized by strongly varying velocities that reach a value up to 5.8 km/s (Figure 10). Taking as reference the crustal velocity structure of China and the Yunnan-Guizhou-Sichuan region (Xiong et al., 1993; Deng et al, 2011; Teng et al., 2013; Zhang E H et al., 2013), Xu et al (2014a) showed that the crystalline basement along the profile corresponds to a velocity about 5.8 km/s and a depth about 2 km and there is a significant undulation in the horizontal direction. It would be the result of the intense regional tectonic activity. The low-velocity zones in the shallowest part of upper crust are located mainly in three regions: the region between YM-LZJF and ANHF, the

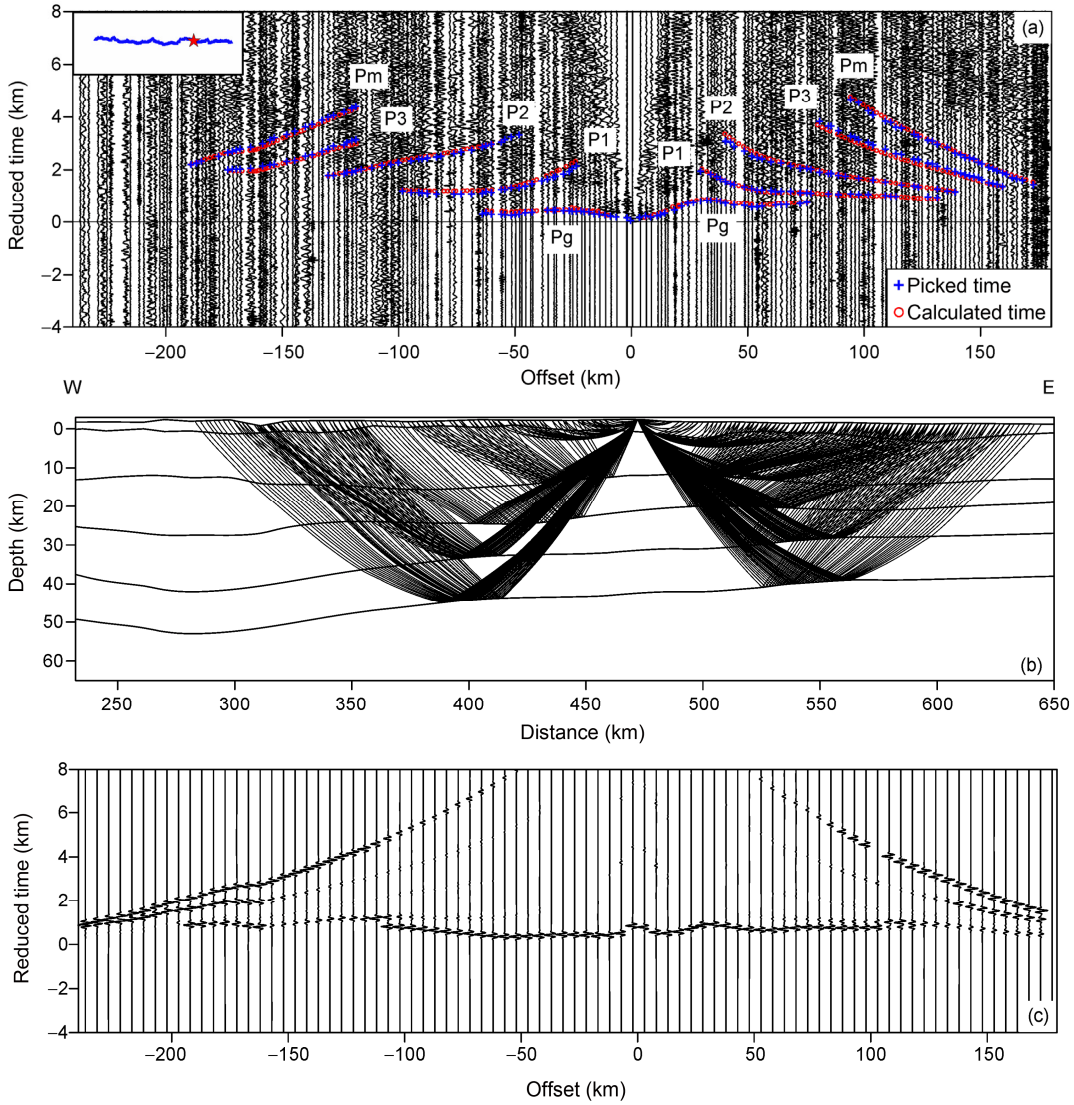

Figure 3 Shot point Sp02 of the Lijiang-Qingzhen profile. Same legend as in Figure 2.

eastern side of XJF, and the east of WN-SCF. The velocities of covering layers in these regions are about 4.0 km/s. A high velocity zone is located to the east of CHF where is the outcrop region of basic and ultrabasic rocks in the inner zone. The velocity in this zone is up to 6.0 km/s.

The average velocity in the middle crust is 6.2–6.6 km/s, and the lateral velocity variation along the profile is significant (Figure 10). The inner zone is characterized by a high-velocity anomaly that locally presents amplitude of about 0.1–0.2 km/s; near the intermediate zone, there are low-velocity characteristics presented in the upper, middle, and lower crusts. The velocity of the lower crust is 6.9–7.2 km/s in the inner zone, and 6.8–7.0 km/s in the intermediate and outer zones (Figure 10).

The depths of the Moho referred in this paper are depths relative to the geoid. In the inner zone the Moho depth along the profile is about 47–53 km; however, the Moho depth is 42–50 km in the intermediate zone and 38–42 km in the outer zone (Figure 10). The Moho depth gradually decreases from the intermediate zone to the outer zone, which has its correspondence in the Bouguer gravity anomaly (Figure 10(a)).

3.2 Comparison of velocities

Based on the velocity distribution in the whole crust, the average velocity is about 6.3–6.5 km/s in the inner zone, 6.2–6.4 km/s in the intermediate zone, and 6.3 km/s in the outer zone (Figure 11). The average velocity is comparatively higher in the inner zone and relatively lower near XJF.

In Figure 12(a) we show the average P-wave velocity of the sedimentary cover along the Lijiang-Qingzhen profile, whereas in Figure 12(b) we show the average velocity of the consolidated continental crust as defined by different velocity contours from 5.8 to 6.1 km/s. The consolidated continental

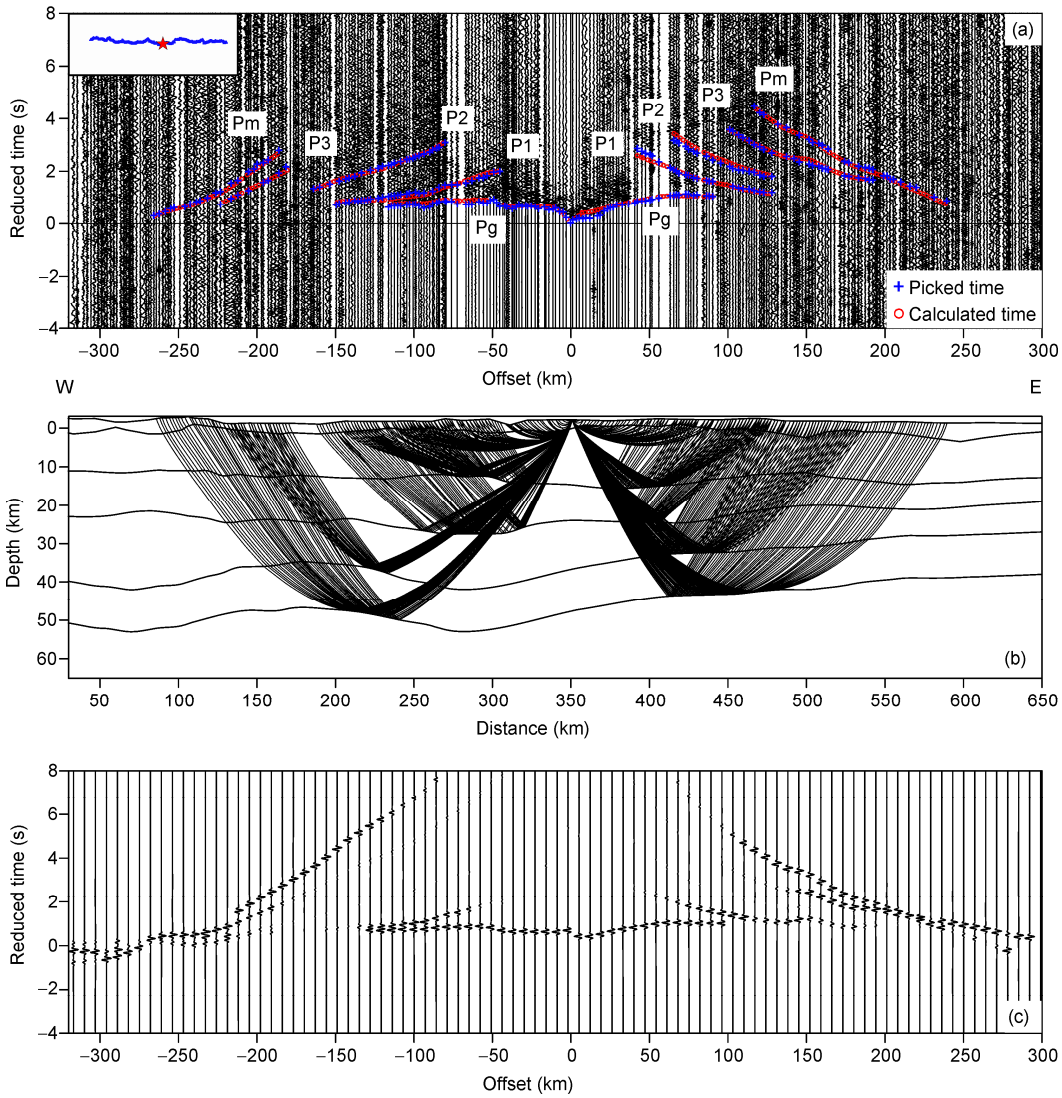

Figure 4 Shot point Sp03 of the Lijiang-Qingzhen profile. Same legend as in Figure 2.

crust makes reference to the part from the crystalline basement to the Moho discontinuity. The results demonstrate that after removing the effect of the cover layer, the average velocity in the inner zone is the largest with a value about 6.4–6.5 km/s, whereas the velocities in the intermediate and outer zones are 6.3–6.4 km/s. Moreover, from a view of the entire profile, the iso-velocity contours within the interval of horizontal distance 100–260 km are very close, but the iso-velocity contours in other regions are further apart. A greater density of contours indicates that near the inner zone, the shallow part of the crust is characterized by less coverage layers with low velocities, larger velocity gradients, and high-velocity anomalies. Correspondingly, there are massive basic and ultrabasic rocks with high velocities outcropping to the surface in this zone.

The average velocity of the whole crust (Figure 11) and the consolidated crust (Figure 12(b)) are relatively lower on both sides of XJF, especially on the east side. Based on the velocity structure of the upper crust (Xu et al., 2014a) and the crustal velocity structure (Figure 10), it is estimated that XJF extends at least down to 40 km depth and maybe even beyond through the crust.

A significant feature of the velocity structure along the profile is that there is a low-velocity thick zone in the upper crust on the east side of XJF, at horizontal distance between 300 and 400 km. This low-velocity zone extends along 100 km and reaches a depth of about 10–15 km in its deeper part. The feature is revealed by the undulated thickness of the sedimentary cover along the Lijiang-Qingzhen profile (Figure 13(a)). In this same illustration (Figure 13(b)), we also can see the variable thickness of the consolidated continental crust as defined by different velocity contours from 5.8 to 6.1 km/s.

4 Discussion

The Lijiang-Panzhihua-Zhehai profile (Xiong et al., 1993)

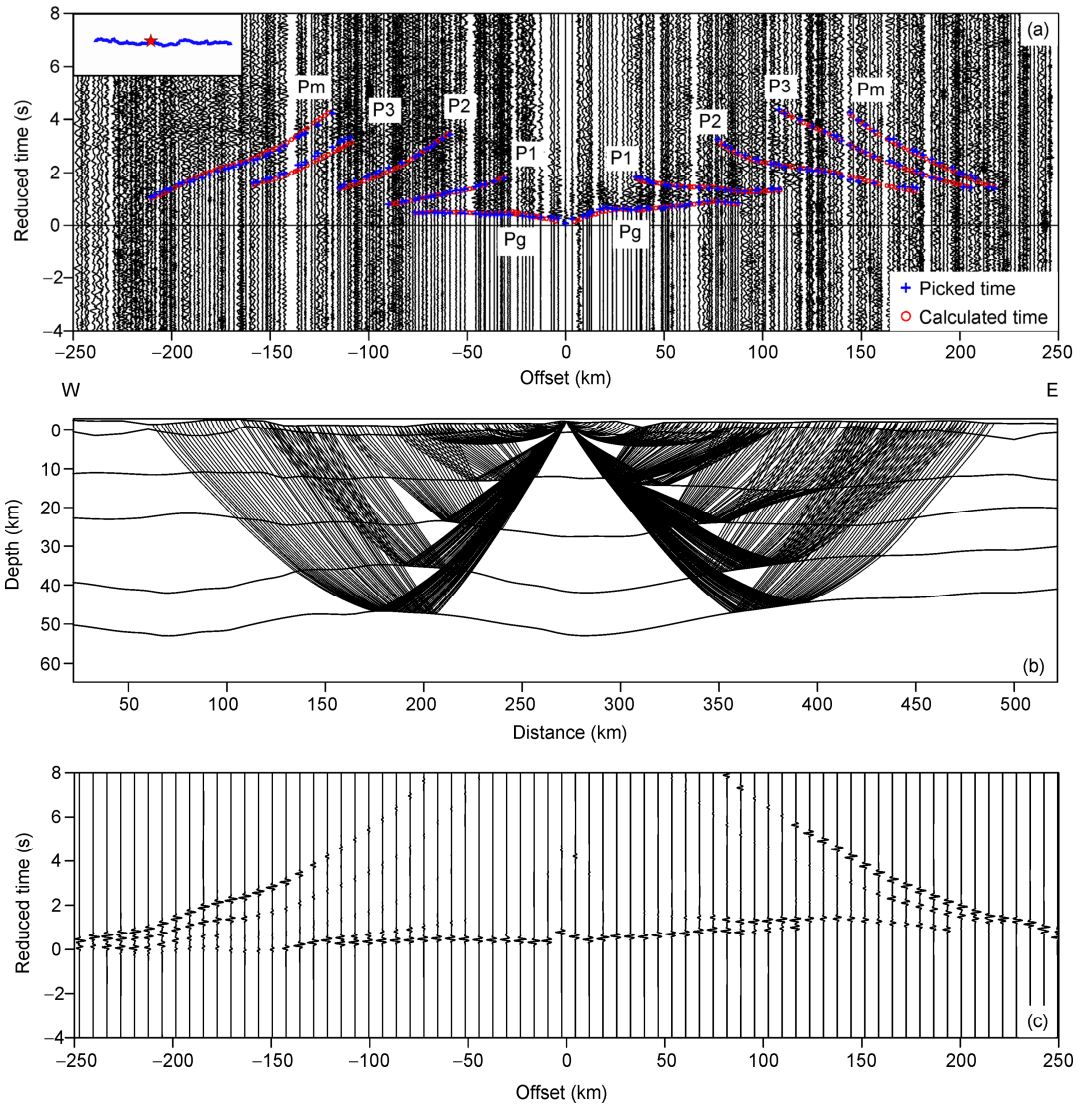

Figure 5 Shot point Sp04 of the Lijiang-Qingzhen profile. Same legend as in Figure 2.

was an active source seismic profile similar to the Lijiang-Panzhihua-Qingzhen profile. The profile was about 360 km long and is overlapped with our profile. The results from the Lijiang-Zhehai profile indicated that there were four low velocity zones and a high velocity zone in the upper crust at the overlap area. The low velocity zones were located in the regions near Lijiang, Yongsheng, between the east of Panzhihua and Huaping and east of Huili, respectively. The high velocity zone was located in the region between Huili and Panzhihua where basic and ultrabasic rocks outcrop on surface. Xiong et al. (1993) thought that this high velocity body was closely related to the metallogenic rocks in Panzhihua. The results above are almost consistent with the fine structure of the upper crust along the Lijiang-Qingzhen profile (Xu et al., 2014a).

There is a low velocity layer with velocity 5.5–5.7 km/s in the middle crust along the Lijiang-Zhehai profile. However, no significant seismic phases were observed along the Lijiang-Qingzhen profile in support of this view. Along the Lijiang-Zhehai profile, the velocity values in the lower crust ranged from 6.6 to 6.8 km/s, and the velocity contours uplifted under the region of Panzhihua, which indicated that the high velocity body in the upper crust at this region might have its origin in a deep tectonic movement (Xiong et al., 1993).

The results from the Lijiang-Qingzhen profile indicate that in the inner zone the velocity is generally higher and the Moho discontinuity uplifts. The results mentioned above are supported by the observation data provided by the permanent/temporary broadband seismic array in the study area. Other studies based on ambient seismic noise show that the S-wave velocity structure presents significant high-velocity anomalies at depth of 10 km in the inner zone (between the shots Sp04 and Sp05) (Liu et al., 2014). There is also an S-wave high-velocity anomaly at 25 km depth in the middle crust (Yao et al., 2008). Moreover, the crust in the inner

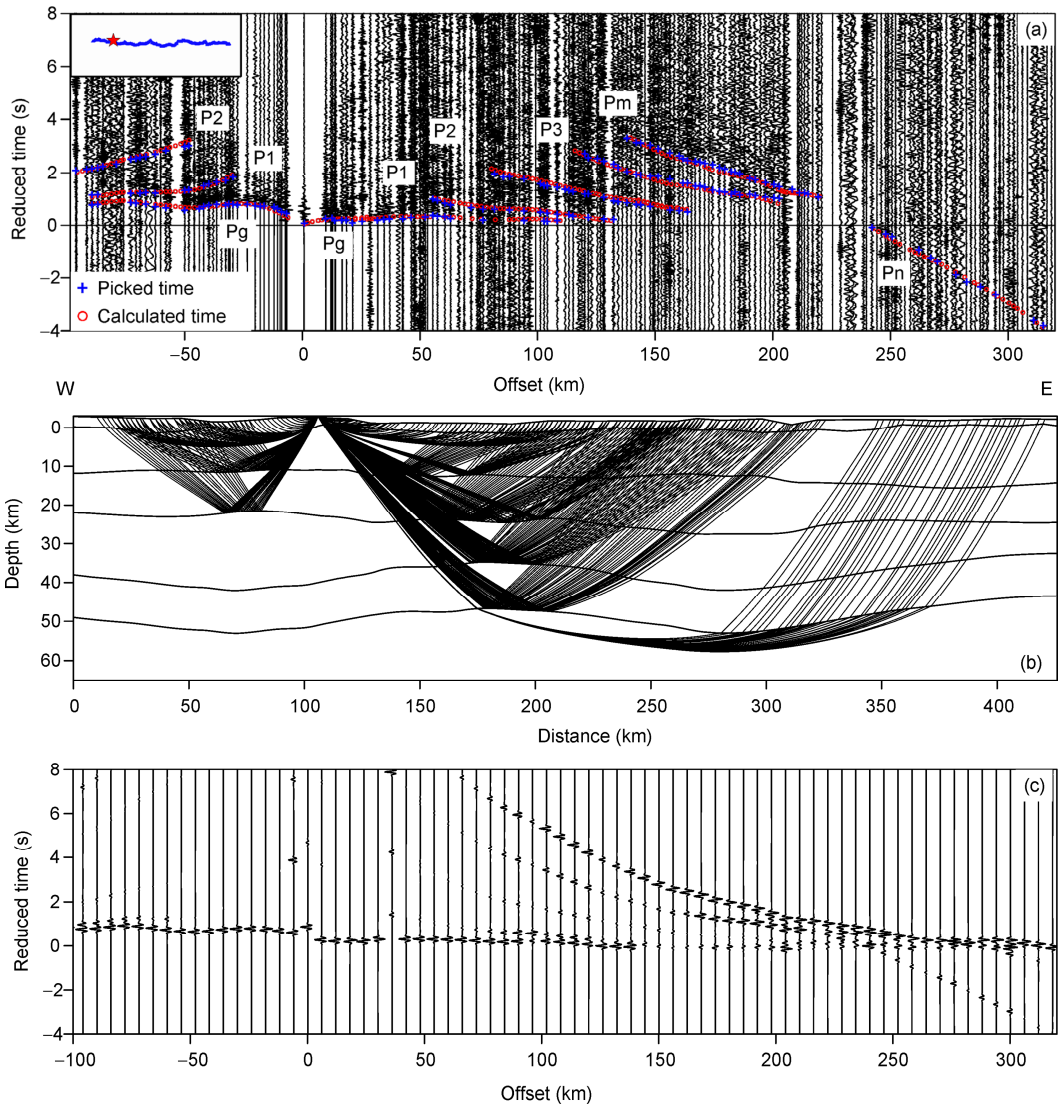

Figure 6 Shot point Sp05 of the Lijiang-Qingzhen profile. Same legend as in Figure 2.

zone is locally characterized by significant S-wave high-velocity anomalies (Zhou et al., 2012). The results obtained by teleseismic body wave tomography indicated that a high-velocity body exists from the bottom of the lower crust to the uppermost mantle and its thickness is about 20 km (Liu et al., 2001). The results supplied by Pn-wave tomography showed a higher velocity in the uppermost mantle in the region of ELIP (Lei et al., 2014).

Receiver function analysis was carried out using high-quality broadband teleseismic waveform data recorded by stations belonging to the Chinese National Digital Seismic Network; the results indicated that the Moho discontinuity in the inner zone uplifts and the depth is 48–58 km between the shots Sp04 and Sp05; to the east of the shots Sp03 and Sp04, the Moho is generally shallower from the inner zone to the intermediate zone and the outer zone and the depth is about 46–48 km (Chen et al., 2010). The Moho depth obtained by the receiver function method is the thickness from the Moho discontinuity to the surface. By removing the impact of the topography, the depth features of the Moho mentioned before are similar to these obtained from wide-angle seismic data. Moreover, the teleseismic receiver function analysis with data recorded by regional stations in Yunnan-Guizhou- Sichuan gave rise to a similar undulation of the Moho depth, although with a more smooth lateral variation (Sun et al., 2012). The comparison of the Moho depth along the Lijiang- Qingzhen profile obtained by different methods is shown in Figure 14. Terrain correction was carried out for all depths and the depths became the thicknesses from the geoid to the Moho discontinuity. The results are different, as can be seen, but all show the same west-east trending.

The Bouguer gravity anomaly increases gradually in ELIP (Figure 10(a)) and the Moho discontinuity is gradually shallower from the inner zone to the outer zone along the profile (Figure 10(b)). The significant feature of the gravity anomaly curve is its uplift in the inner zone (Deng et

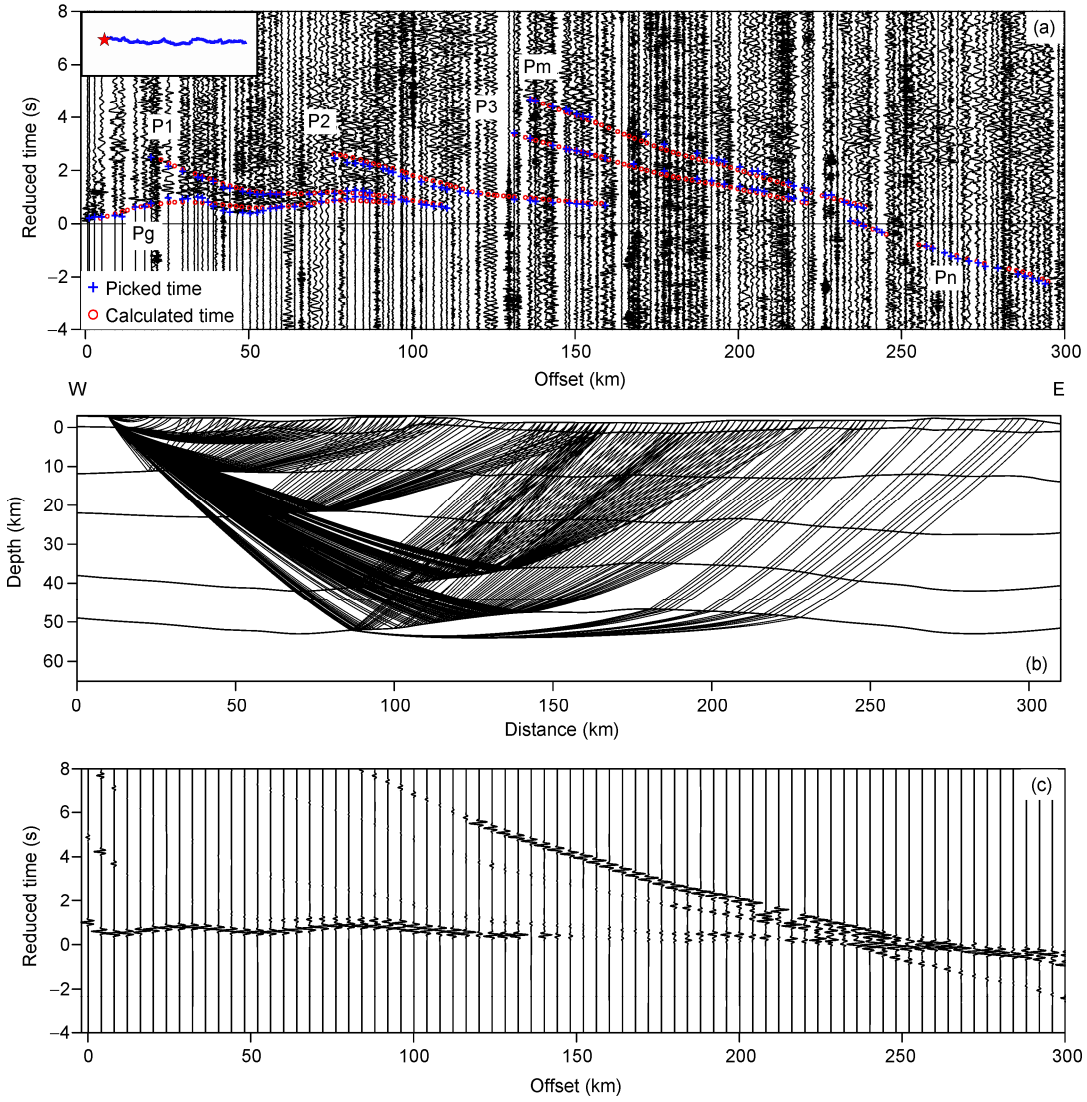

Figure 7 Shot point Sp06 of the Lijiang-Qingzhen profile. Same legend as in Figure 2.

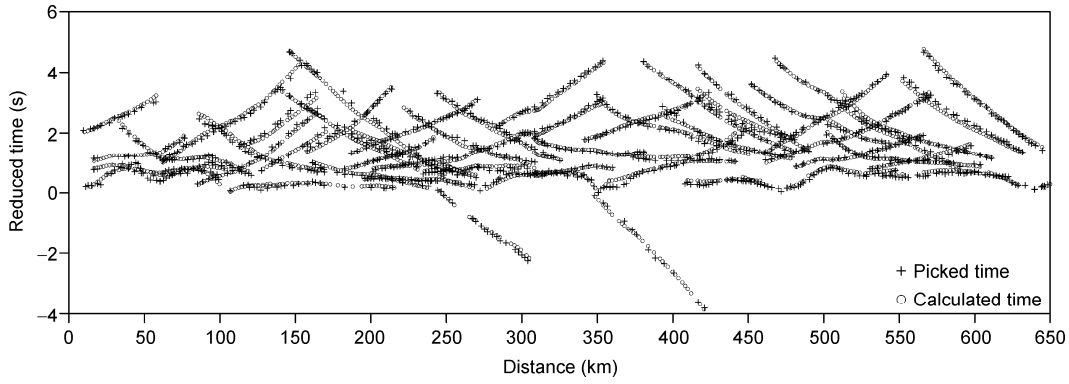

Figure 8 Observed (crosses) and calculated (circles) travel times for all P-phases recorded from the six shots fired along the Lijiang-Qingzhen profile revealing a good agreement.

al., 2014). This indicates some features of the deep structure in the inner zone: high-density anomalies exist in the crust, which correspond with the seismic high velocity anomalies or the Moho depth variation. The features of the velocity model from the gravity observation are consistent with those of the velocity model here determined.

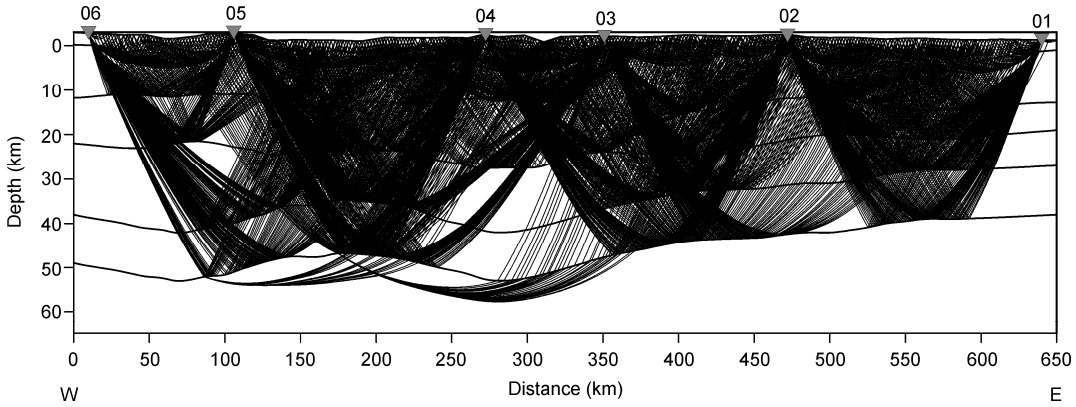

Figure 9 Ray coverage diagram for the six shots fired along the Lijiang-Qingzhen profile that allows seeing the illumination of the crust. Inverted triangles on top mark the shot points.

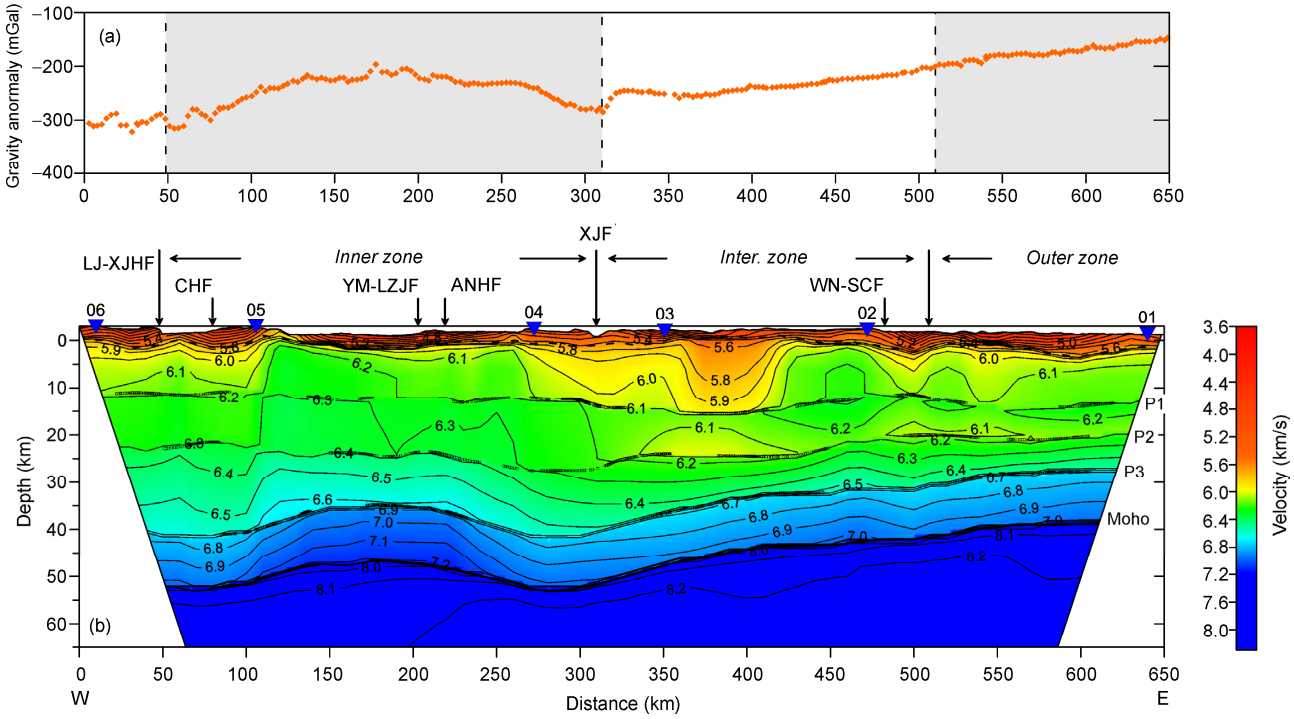

Figure 10 Bouguer gravity anomaly (a) and 2D seismic velocity structure of the crust (b) along the Lijiang-Qingzhen profile. Intra-crustal reflectors (P1, P2, P3) and the Moho discontinuity are drawn following the reflection points of the ray paths (small circles). Shot points (inverted blue triangles), regional faults (arrows with head down), and the three zones in which ELIP is conventionally divided are indicated on top in agreement with the nomenclature expressed in caption of Figure 1.

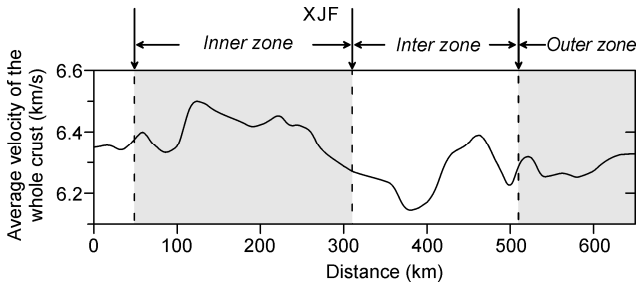

Figure 11 Average P-wave velocity of the whole crust beneath the Lijiang-Qingzhen profile. The vertical dashed lines divide the profile into the inner, intermediate, and outer zones; XJF is the acronym for the Xiaojiang fault.

From the gravity curve (Figure 10(a)), the range of the gravity anomaly (wavelength) in the inner zone is ~250 km (between 50 and 300 km). There is an empirical relationship between the range of the density anomaly (z) and the range of the observed gravity anomaly (wavelength λ), which is $\lambda \approx 2\pi z$ (Artemieva, 2011). On the basis of this relationship, we can deduce $z \approx 40$ km, which indicates that the gravity anomaly in the inner zone is the product of the density anomaly on crustal scale, including the topography of the Moho discontinuity. Based on the generally positive correlation between crustal density and seismic velocity, the above result provides a support to our velocity model.

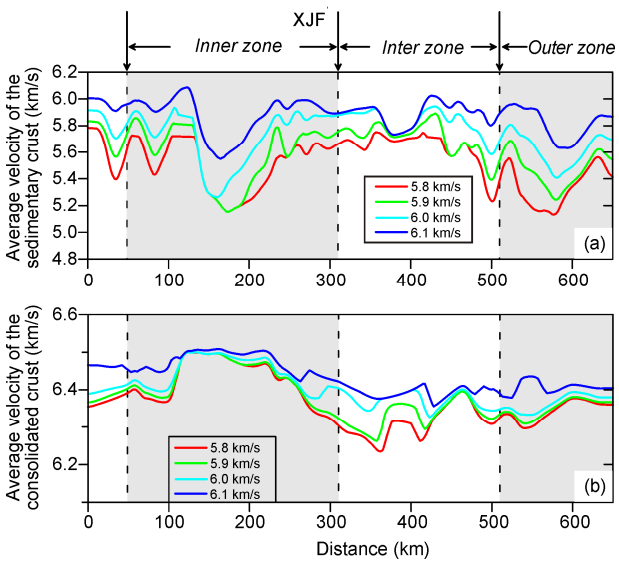

Figure 12 Average P-wave velocity of the sedimentary cover (a) and the consolidated continental crust (b) as defined by different velocity contours from 5.8 to 6.1 km/s along the Lijiang-Qingzhen profile. The consolidated continental crust makes reference to the part from the crystalline basement to the Moho discontinuity. XJF is the acronym for the Xiaojiang fault.

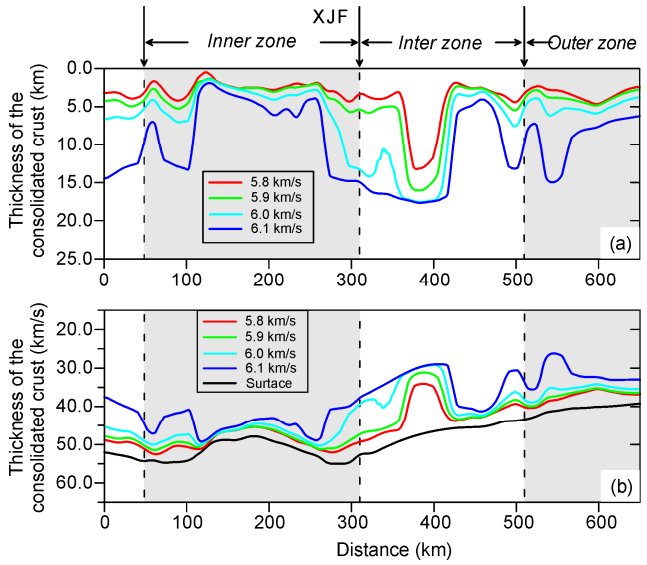

Figure 13 Thickness of the sedimentary cover (a) and the consolidated continental crust (b) as defined by different velocity contours from 5.8 to 6.1 km/s along the Lijiang-Qingzhen profile. XJF is the acronym for the Xiaojiang fault.

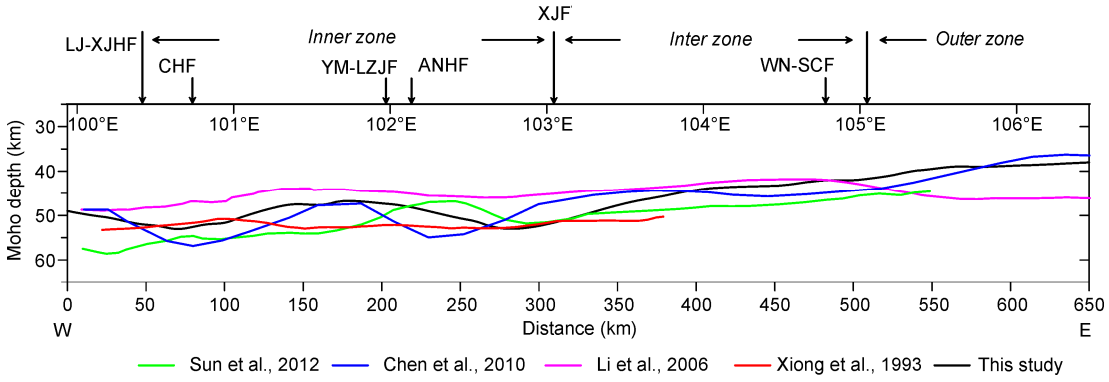

Figure 14 The Moho depth along the Lijiang-Qingzhen profile compared with the depth obtained in previous studies (Xiong et al., 1993; Li et al., 2006; Chen et al., 2010; Sun et al., 2012) and this study. Regional faults (arrows with head down) and the three zones in which ELIP is conventionally divided are indicated on top in agreement with the nomenclature expressed in caption of Figure 1.

5 Evidence of an ancient mantle plume

The erosive volume of uplifted crust is the largest in the inner zone of the ELIP (He et al., 2003a, 2003b). From bottom to top, the basalt rocks there vary from low-Ti lavas to high-Ti lavas, and the picrites are locally distributed (Zhang et al., 2006b; Zhang Y et al., 2013). However, we also found high-Ti lavas in the intermediate zone. Low-Ti lavas are formed with a high degree of partial melting of the mantle, whereas high-Ti lavas are formed with a small degree. Based on features of the dome-shaped uplift of the crust and the spatial distribution of the basalts, the inner zone of the ELIP is interpreted as the impact site of an ancient mantle plume head (Xu Y G et al., 2004; Deng et al., 2014). In the inner zone, a high degree of partial melting of the mantle led to the formation of voluminous magmas. Part of these magmas erupted toward the surface, and the other part remained at different depths of the crust in the form of intrusive rocks and magmatic underplating. These mafic basalts could be recognized in the seismic velocity structure. In the inner zone of the ELIP the Moho discontinuity is characterized by local uplift (Figure 10) and the consolidated continental crust presents high P-wave velocity anomalies (Figures 10–12(b)), which may be the imprint of magma intrusion and underplating. The melting of a mantle plume would generate picritic magmas with about ~20% MgO (Zhang et al., 2006b; Zhang Y et al., 2013), which are characterized by a great density. When the picritic magmas rise to the Moho, their density was higher than that of the surrounding crust. As a consequence of this density contrast,

magmas are trapped at the Moho boundary and the magmatic underplating occurred. In the course of magmatic underplating highly magnesium magmas experience fractional crystallization and the minerals including spinels, olivines, and clinopyroxenes tend to be accumulated on the bottom of the lower crust. Residual magmas subsequent to intensive fractionation will have low density and gain their buoyancy to rise to the upper levels of the crust. It is possible that similar processes would appear many times through development of magma chamber or intraplating during magma ascent to the surface. These processes explain why the majority of flood basalts are strongly fractionated rather than being primitive. This is further supported by the high-velocity anomalies in the crust (Figure 10; Farnetani et al., 1996; Xu Y G et al., 2004, 2013; Xu and He, 2007). In the inner zone of the ELIP, the Moho is characterized by a local uplift (Figure 10) that might be caused by the uplift of the ascending plume head. The resulting magmatic underplating could cause the thinning of the crust so that the space so generated was rapidly filled by the inflow of magma.

6 Conclusions

We have obtained the crustal velocity structure along the Lijiang-Qingzhen profile on the basis of the data acquired through an active source wide-angle seismic experiment. The middle crust in the inner zone is characterized by high-velocity anomalies, with the average velocity of 6.2–6.6 km/s, which is about 0.1–0.2 km/s higher than the normal one. The velocity of the lower crust in the inner zone is 6.9–7.2 km/s, higher than those observed in the intermediate and outer zones (6.7–7.0 km/s). The depth to the Moho discontinuity decreases gradually from 47–53 km in the inner zone, via 42–50 km in the intermediate zone to 38–42 km in the outer zone. In the inner zone of ELIP, the Moho is characterized by local uplift and the consolidated continental crust presents high P-wave velocity anomalies, which may be the imprint of magma intrusion and underplating caused by the Permian mantle plume. Of course, the results presented here are preliminary and still need to be complemented with other geophysical studies in order to obtain more information on the V_p/V_s ratio, density, anisotropy, rheology, and magnetism, and thus provide new constraints on the lithosphere.

We thank the group of the Geophysical Exploration Central, China Earthquake Administration and all workers of the Institute of Geology and Geophysics, Chinese Academy of Sciences, who made possible the field seismic data acquisition. We are very grateful to Professor José Badal for his assistance during the preparation and revision of the original manuscript. We thank Professors Fuyun Wang and Shixu Jia for their guidance and assistance. Helpful discussions and suggestions from Associate Professors Chenglai Miao and Zhiming Bai are sincerely acknowledged. Also, we thank three anonymous reviewers for their constructive comments, which have greatly improved the quality of this paper. This study was supported by the National Basic Research Program of China (Grant No. 2011CB808904) and the National Natural Science Foundation of China (Grants Nos. 41274070, 41474068).

Ali J R, Thompson G M, Zhou M F, et al. 2005. Emeishan large igneous province, SW China. Lithos, 79: 475–489
Armijo R, Tapponnier P, Han T L. 1989. Late Cenozoic right-lateral strike-slip faulting in southern Tibet. J Geophys Res, 94(B3): 2787–2838
Artemieva I M. 2011. The Lithosphere: An Interdisciplinary Approach, Chapter 6.4. Cambridge: Cambridge University Press
Bai Z M, Wang C Y. 2003. Tomographic investigation of the upper crustal structure and seismotectonic environments in Yunnan Province (in Chinese). Acta Seismol Sin, 25: 117–127
Campbell I H. 2001. Identification of ancient mantle plumes. Geol Soc Am Sp P, 352: 5–21
Campbell I H, Griffiths R W. 1990. Implications of mantle plume structure for the evolution of flood basalts. Earth Planet Sci Lett, 99: 79–93
Cerveny V. 2001. Seismic Ray Theory. Cambridge: Cambridge University Press
Červený V, Klimeš L, Pšenčík I. 1988. Complete seismic-ray tracing in three-dimensional structures. In: Doornbos D J, ed. Seismological Algorithms. New York: Academic Press. 89–168
Chen Y, Zhang Z J, Sun C Q, et al. 2013. Crustal anisotropy from Moho converted Ps wave splitting analysis and geodynamic implications beneath the eastern margin of Tibet and surrounding regions. Gondwana Res, 24: 946–957
Chen Y L, Niu F L, Liu R F, et al. 2010. Crustal structure beneath China from receiver function analysis. J Geophys Res, 115: B03307
Christensen N I, Mooney W D. 1995. Seismic velocity structure and composition of the continental crust: A global view. J Geophys Res, 100(B7): 9761–9788
Chung S L, Jahn B M. 1995. Plume-lithosphere interaction in generation of the Emeishan flood basalts at the Permian-Triassic boundary. Geology, 23: 889–892
Coffin M F, Eldholm O. 1994. Large igneous provinces: Crustal structure, dimensions, and external consequences. Rev Geophys, 32: 1–36
Courtillot V, Davaille A, Besse J, et al. 2003. Three distinct types of hotspots in the Earth's mantle. Earth Planet Sci Lett, 205: 295–308
Courtillot V, Jaupart C, Manighetti I, et al. 1999. On causal links between flood basalts and continental breakup. Earth Planet Sci Lett, 166: 177–195
Deng Y F, Li S L, Fan W M, et al. 2011. Crustal structure beneath South China revealed by deep seismic soundings and its dynamics implications (in Chinese). Chin J Geophys, 54: 2560–2574
Deng Y F, Zhang Z J, Mooney W, et al. 2014. Mantle origin of the Emeishan large igneous province (South China) from the analysis of residual gravity anomalies. Lithos, 204: 4–13
Farnetani C G, Richards M A, Ghiorso M S. 1996. Petrological models of magma evolution and deep crustal structure beneath hotspots and flood basalt provinces. Earth Planet Sci Lett, 143: 81–94
He B, Xu Y G, Chung S L, et al. 2003a. Sedimentary evidence for a rapid, kilometer-scale crustal doming prior to the eruption of the Emeishan flood basalts. Earth Planet Sci Lett, 213: 391–405
He B, Xu Y G, Xiao L, et al. 2003b. Generation and spatial distribution of the Emeishan Large Igneous Province: New evidence from stratigraphic records (in Chinese). Acta Geol Sin, 77: 194–202
He B, Xu Y G, Huang X L, et al. 2007. Age and duration of the Emeishan flood volcanism, SW China: Geochemistry and SHRIMP zircon U-Pb dating of silicic ignimbrites, post-volcanic Xuanwei Formation and clay tuff at the Chaotian section. Earth Planet Sci Lett, 255: 306–323
He B, Xu Y G, Wang Y M, et al. 2005. The magnitude of crustal uplift prior to the eruption of the Emeishan basalt: Inferred from sedimentary records. Geotect Metall, 29: 316–320
He B, Xu Y G, Wang Y M, et al. 2006a. Sedimentation and lithofacies paleogeography in southwestern China before and after the Emeishan flood volcanism: New insights into surface response to mantle plume activity. J Geol, 114: 117–132

He B, Xu Y G, Xiao L, et al. 2006b. Sedimentary responses to uplift of Emeishan mantle plume and its implications (in Chinese). Geolog Rev, 52: 30–37
He H L, Fang Z J, Li P. 1993. A preliminary approach to the fault activity of southern segment on Xiaojiang west branch fault. J Seismol Res, 16: 291–298
He H L, Yasutakyr I. 2007. Faulting on the Anninghe fault zone, Southwest China in late Quaternary and its movement model. Acta Seismol Sin, 29: 537–548
Hole J A. 1992. Nonlinear high resolution three dimensional seismic travel time tomography. J Geophys Res, 97(B5): 6553–6562
Lan H Q, Zhang Z J. 2013a. Topography-dependent eikonal equation and its solver for calculating first-arrival traveltimes with an irregular surface. Geophys J Int, 193: 1010–1026
Lan H Q, Zhang Z J. 2013b. A High-order fast-sweeping scheme for calculating first-arrival travel times with an irregular surface. Bull Seismol Soc Am, 103: 2070–2082
Lan H Q, Zhang Z, Xu T, et al. 2012a. A comparative study on the fast marching and fast sweeping methods in the calculation of first-arrival traveltime field (in Chinese). Progr Geophys, 27: 1863–1870
Lan H Q, Zhang Z, Xu T, et al. 2012b. Effects due to the anisotropic stretching of the surface-fitting grid on the traveltime computation for irregular surface by the coordinate transforming method (in Chinese). Chin J Geophys, 55: 3355–3369
Lei J S, Zhao D P. 2006. A new insight into the Hawaiian plume. Earth Planet Sci Lett, 241: 438–453
Lei J S, Li Y, Xie F R, et al. 2014. Pn anisotropic tomography and dynamics under eastern Tibetan plateau. J Geophy Res-Solid Earth, 119: 2174–2198
Li F, Xu T, Wu Z B, et al. 2013. Segmentally iterative ray tracing in 3-D heterogeneous geological models (in Chinese). Chin J Geophys, 56: 3514–3522
Li S L, Mooney W D, Fan J C. 2006. Crustal structure of mainland China from deep seismic sounding data. Tectonophysics, 420: 239–252
Liu J H, Liu F T, He J K, et al. 2001. Study of seismic tomography in Panxi paleorift area of Southwestern China-structural features of crust and mantle and their evolution. Sci China Ser D-Earth Sci, 44: 277–288
Liu Q Y, van der Hilst R D, Li Y, et al. 2014. Eastward expansion of the Tibetan Plateau by crustal flow and strain partitioning across faults. Nature Geosci, 7: 361–365
Liu Y F, Lan H Q. 2012. Study on the numerical solutions of the eikonal equation in curvilinear coordinate system (in Chinese). Chin J Geophys, 55: 2014–2026
Lo C H, Chung S L, Lee T Y, et al. 2002. Age of the Emeishan flood magmatism and relations to Permian-Triassic boundary events. Earth Planet Sci Lett, 198: 449–458
Ma T, Zhang Z J. 2014. Calculating ray paths for first-arrival travel times using a topography-dependent eikonal equation solver. Bull Seismol Soc Am, 104: 1501–1517
Peate I U, Bryan S E. 2008. Re-evaluating plume-induced uplift in the Emeishan large igneous province. Nature Geosci, 1: 625–629
Qiao X J, Wang Q, Du R L. 2004. Characteristics of current crustal deformation of active blocks in the Sichuan-Yunnan region (in Chinese). Chin J Geophys, 47: 805–811
Richards M A, Duncan R A, Courtillot V E. 1989. Flood basalts and hot-spot tracks: Plume heads and tails. Science, 246: 103–107
Sun Y, Niu F L, Liu H F, et al. 2012. Crustal structure and deformation of the SE Tibetan plateau revealed by receiver function data. Earth Planet Sci Lett, 349-350: 186–197
Teng J W. 1994. Lithospheric Physics and Dynamics of Kang-dian Tectonic Zone (in Chinese). Beijing: Sciences Press
Teng J W, Zhang Z J, Zhang X K, et al. 2013. Investigation of the Moho discontinuity beneath the Chinese mainland using deep seismic sounding profiles. Tectonophysics, 609: 202–216
Vidale J. 1988. Finte-difference calculation of travel times. Bull Seismol Soc Am, 78: 2062–2076
Wang C Y, Mooney W D, Wang X L, et al. 2002. Study on 3-D velocity structure of crust and upper mantle in Sichuan and Yunnan region, China (in Chinese). Acta Seismol Sin, 24: 1–16
Wignall P B, Sun Y D, Bond D P G, et al. 2009. Volcanism, mass extinction and carbon isotope fluctuations in the Middle Permian of China. Science, 324: 1179–1182
Wu J, Zhang Z J. 2012. Spatial distribution of seismic layer, crustal thickness, and *Vp*/*Vs* ratio in the Permian Emeishan mantle plume region. Gondwana Res, 22: 127–139
Wu P, Liu S F, Dou G X. 2014. Sedimentary response to Emeishan mantle plume in the eastern Yunnan Province. Acta Petrol Sin, 30: 1793–1803
Xia L Q, Xia Z C, Xu X Y, et al. 2004. Carboniferous Tianshan igneous megaprovince and mantle plume (in Chinese). Geolog Bull China, 23: 903–910
Xiang H F, Xu Y W, Guo S M, et al. 2002. Sinistral thrusting along the Lijiang-Xiaojinhe fault since Quaternary and its geological-tectonic significance-Shielding effect of transverse structure of intracontinental active block (in Chinese). Seismol Geol, 24: 188–198
Xiong S B, Zheng Y, Yin Z X, et al. 1993. The 2-D structure and it's tectonic implications of the crust in the Lijiang-Pan Zhihua-Zhehai region (in Chinese). Chin J Geophys, 36: 434–444
Xu T, Xu G M, Gao E G, et al. 2006. Block modeling and segmentally iterative ray tracing in complex 3D media. Geophysics, 71: T41–T51
Xu T, Xu G M, Gao E G, et al. 2004. Block modeling and shooting ray tracing in complex 3D media (in Chinese). Chin J Geophys, 47: 1118–1126
Xu T, Zhang Z J, Gao E G, et al. 2010. Segmentally iterative ray tracing in complex 2D and 3D heterogeneous block models. Bull Seismol Soc Am, 100: 841–850
Xu T, Zhang M H, Tian X B, et al. 2014a. Upper crustal velocity of Lijiang-Qingzhen profile and its relationship with the seismogenic environment of the M_s6.5 Ludian earthquake (in Chinese). Chin J Geophys, 57: 3069–3079
Xu T, Li F, Wu Z B, et al. 2014b. A successive three-point perturbation method for fast ray tracing in complex 2D and 3D geological model. Tectonophysics, 627: 72–81
Xu Y G. 2002. Mantle plumes, large igneous provinces and their geologic consequences (in Chinese). Earth Science Frontiers, 9: 341–353
Xu Y G, Chung S L. 2001. The Emeishan large igneous province: Evidence for mantle plume activity and melting conditions (in Chinese). Geochimica, 30: 1–9
Xu Y G, Chung S L, Jahn B, et al. 2001. Petrologic and geochemical constraints on the petrogenesis of Permian-Triassic Emeishan flood basalts in southwestern China. Lithos, 58: 145–168
Xu Y G, He B, Chung S L, et al. 2004. Geologic, geochemical, and geophysical consequences of plume involvement in the Emeishan flood-basalt province. Geology, 32: 917–920
Xu Y G, He B, Huang X L, et al. 2007a. The debate over mantle plumes and how to test the plume hypothesis (in Chinese). Earth Science Frontiers, 14: 001–009
Xu Y G, He B, Huang X, et al. 2007b. Identification of mantle plumes in the Emeishan Large Igneous Province. Episodes, 30: 32–42
Xu Y G, He B, Luo Z Y, et al. 2013. Study on mantle plume and large igneous provinces in China: An overview and perspectives (in Chinese). Bull Mineral Petrol Geochem, 32: 25–39
Yao H J, Beghein C, Van der Hilst, R D. 2008. Surface-wave array tomography in SE Tibet from ambient seismic noise and two-station analysis-II. Crustal and upper-mantle structure. Geophys J Int, 173: 205–219
Zelt C A, Smith R B. 1992. Seimic traveltime inversion for 2-D crustal velocity structure. Geophys J Int, 108: 16–34
Yu W X, Liu Y Q, He W. 1997. Characters of recent crustal deformation and earthquakes on the Xiaojiang fault zone in Yunnan Province (in Chinese). Seismol Geol, 19: 17–21
Zhang E H, Lou H, Jia S X, et al. 2013. The deep crust structure characteristics beneath western Yunnan (in Chinese). Chin J Geophys, 56: 1915–1927
Zhang R Q, Zhou Y, Wang X W, et al. 2009. Structural features and tectonic evolution of the Wei-Zi-Luo fault zone in southwestern Guizhou province (in Chinese). J Geomechan, 15: 178–189
Zhang Y, Ren Z Y, Xu Y G. 2013. Sulfur in olivine-hosted melt inclusions of Emeishan picrites: Implications for S degassing and its impact on environment. J Geophys Res, 118: 1–8

Zhang Z C, Dong S Y. 2007. Were large igneous provinces caused by mantle plumes? (in Chinese). Geoscience, 21: 247–254
Zhang Z C, Mahoney J J, Wang F S, et al. 2006a. Geochemistry of picritic and associated basalt flows of the western Emeishan flood basalt province, China: Evidence for a plume-head origin (in Chinese). Acta Petrol Sin, 22: 1538–1552
Zhang Z C, Mahoney J J, Mao J W, et al. 2006b. Geochemistry of picritic and associated basalt flows of the western Emeishan flood basalt province, China. J Petrol, 47: 1997–2019
Zhang Z J, Deng Y F, Chen L, et al. 2013. Seismic structure and rheology of the crust under mainland China. Gondwana Res, 23: 1455–1483
Zhao A H, Zhang Z J, Teng J W. 2004. Minimum travel time tree algorithm for seismic ray tracing: Improvement in efficiency. J Geophys Eng, 1: 245–251
Zhao F F, Ma T, Xu T. 2014. A review of the travel-time calculation methods of seismic first break (in Chinese). Progr Geophys, 29: 1102–1113
Zhou L Q, Xie J Y, Shen W S, et al. 2012. The structure of the crust and uppermost mantle beneath South China from ambient noise and earthquake tomography. Geophys J Int, 189: 1565–1583
Zhou M F, Malpas J, Song X Y, et al. 2002. A temporal link between the Emeishan large igneous province (SW China) and the end-Guadalupian mass extinction. Earth Planet Sci Lett, 196: 113–122
Zhong Y T, He B, Mundil R, et al. 2014. CA-TIMS zircon U-Pb dating of felsic ignimbrite from the Binchuan section: Implications for the termination age of Emeishan large igneous province. Lithos, 204: 14–19
Zhu B Q, Chang X Y, Hu Y G, et al. 2002. Discovery of Yanhe copper deposit in the Yunnan-Guizhou border area and a new train of thought for copper prospecting in the large igneous province of Emeishan flood basalts (in Chinese). Adv Earth Sci, 17: 912–917